A Fast and Robust Open-Switch Fault Diagnosis Method for Variable-Speed PMSM System

Xinxiu Zhou, *Member, IEEE*, Jun Sun, Peiling Cui, *Member, IEEE*, Yanhua Lu, Ming Lu, and Yang Yu

***Abstract*—Traditional open-switch fault diagnosis methods suffer from poor rapidity or robustness. To solve this issue, a new differential current observer-based fault diagnosis method is proposed in this article. With the designed differential observer, fault symptoms (residuals) can be generated and adopted for fault diagnosis easily. Considering that the residuals are sensitive to motor operating condition in the conventional model-based method due to model error, an adaptive fault detection threshold is designed. As a result, the false detection and missed detection caused by the change of working condition can be avoided, and stronger robustness against speed, load, and parameter variations can be achieved with superior rapidity compared with existing methods. Finally, the rapidity and robustness of the proposed fault diagnosis method are verified sufficiently through experimental results.**

***Index Terms*—Fault diagnosis, observer, permanent magnet motors, pulsewidth modulation (PWM) invertor.**

NOMENCLATURE

u_{xo}	Terminal voltage.
$\bar{u}_{xo}$	Average terminal voltage in every PWM period.
u^*_{xo}	Terminal voltage command given by current loop.
Δu_{xo}	Terminal voltage distortion.
u_{xn}	Phase voltage.
$u_{xn}{}^*$	Phase voltage command given by current loop.
u_j	Actual equivalent input.
$\hat{u}_j$	Estimated equivalent input.
$\boldsymbol{u}$	Estimated equivalent input vector.
Δu_j	Differential voltage distortion.
$\boldsymbol{u_f}$	Differential voltage distortion vector.
i_x	Phase current.
i^*_x	Phase current reference.
i_j	Differential current.
Δi_j	Forward difference of i_j.
$\hat{i}_j$	Estimated differential current.
$\boldsymbol{i}$	Differential current vector.
Δi_j	Differential current distortion.
r_j	Residual.
$\boldsymbol{r}$	Residual vector.
$\boldsymbol{r_n}$	Normalized residual vector.
$\boldsymbol{r_{nk}}$	Ideal normalized residual vector after fault.
z_p	Closed-loop pole of the observer.
M_r	Modulus of residual vector/fault detection index.
T_{h1}	First adaptive fault detection threshold.
T_{h2}	Second adaptive fault detection threshold.
F	Fault status flag.
P	Fault source indicator.

Manuscript received May 8, 2020; revised June 27, 2020; accepted July 27, 2020. Date of publication August 3, 2020; date of current version October 30, 2020. This work was supported by the National Natural Science Foundation of China under Grants 61873020 and 61673044. Recommended for publication by Associate Editor J. Ye. *(Corresponding author: Peiling Cui.)*

Xinxiu Zhou and Peiling Cui are with the Research Institute for Frontier Science, Beihang University, Beijing 100191, China (e-mail: 580927@163.com; cuiplhh@126.com).

Jun Sun is with the School of Instrumentation and Optoelectronic Engineering, Beihang University, Beijing 100191, China (e-mail: junsunbuaa@qq.com).

Yanhua Lu is with the Shanghai Aerospace Control Technology Institute, Shanghai 201109, China (e-mail: luyi0303@163.com).

Ming Lu is with the Beijing Institute of Control Engineering, Beijing 100190, China (e-mail: lmuing@hotmail.com).

Yang Yu is with the Faulty of Engineering and Information Technology, University of Technology Sydney, Sydney, NSW 201101, Australia (e-mail: yang.yu@uts.edu.au).

Color versions of one or more of the figures in this article are available online at https://ieeexplore.ieee.org.

Digital Object Identifier 10.1109/TPEL.2020.3013628

I. INTRODUCTION

THE permanent magnet synchronous motor (PMSM) has been widely applied in various applications such as aircraft, automotive, and transportation, which require high reliability [1]–[5]. However, unpredictable faults may occur in the PMSM drives. It is found that almost 70% of faults in the drives relate to power switches (short/open-switch faults) [6]. Therefore, a power switch fault diagnosis is a critical issue in practice. Generally, the short-switch fault is hard to be detected by the software, thus hardware detection and protection circuits are utilized to avoid motor damage [7]. With the protection circuits, the short-circuit switch is turned OFF, and the short-circuit fault turns to an open-switch fault. As for the open-switch fault, it may lead to motor phase current distortion and torque fluctuation. Hence, fast and reliable open-switch fault diagnosis is not a trivial task but worth studying.

Recently, various voltage source inverter (VSI) open-switch fault diagnosis methods have been proposed. According to the information required for residual generation, these methods can be classified into voltage-based method [8]–[15], current-based method [16]–[23], and model-based method [24]–[30]. In the voltage-based methods, residuals are obtained by comparing the voltage reference values with their measured values, and those voltages include instant bridge arm pole voltages [8] [9], instant bridge arm pole-to-pole voltages [10]–[13], or gate voltages [14], [15]. These methods possess fast detection speed. But, additional hardware is required for detecting the voltage, which increases the system cost, volume, and complexity. As for the current-based method, it generates residuals from motor currents

indexes, including current vector [16]–[19], average current [20], current reference error [21], [22], and near-zero current [23]. As the current information is available in most of the motor control systems, extra hardware can be avoided in this kind of fault diagnosis method. Besides, improved robustness against load variation can be obtained owing to the current index's normalizations. Nevertheless, a large time delay (at least one electrical period) is induced by the current index's calculation. As a result, the current-based fault diagnosis method presents poor rapidity.

For fast diagnosis without additional hardware, model-based methods are proposed in [24]–[30]. In these methods, motor models are employed to estimate motor voltage/current variables (or their derivation indicators), and the residuals are obtained by comparing the reference/measured values with their estimated values. These model-based methods can be divided into voltage observer-based methods [24], [25] and current observer-based methods [26]–[30]. Although the voltage observer-based methods possess the advantage of rapidity, its anti-interference ability is limited. For better anti-interference performance, the current observer-based methods are proposed in [26]–[30]. In [26], switch open fault is diagnosed based on a decoupled closed-loop current observer. Its fault detection time is acceptable, but it requires quite a long time for fault isolation (about five electrical periods). Noticed that the fault diagnosis mainly includes fault detection and fault isolation (FDI) two steps, both steps will affect the total fault diagnosis time. It is necessary to find a decent solution to reduce the FDI time simultaneously.

In [27], the fault isolation time is greatly shortened by judging the residual vector direction. Nevertheless, at least one electrical period is required for the whole fault diagnosis. In [28], a mixed logical dynamic (MLD) model of the motor drive system is employed to estimate the motor three-phase currents and to generate the currents residuals vector. With the MLD model, fault diagnosis finishes within a quarter of the electrical period. However, the fixed fault detection threshold makes its robustness inferior. In [29], the *d*–*q* currents observer is used to realize fault diagnosis in permanent-magnet synchronous generators drives. Especially, this method shows fair robustness against load variation by utilizing the current form factors (variables insensitive to load variation) as fault detection indexes. However, the fixed fault detection threshold obtained by cut-and-trail reduces the reliability of fault diagnosis results, which also makes the algorithm more difficult to implement. After that, an improved method with an adaptive fault detection threshold is introduced in [30]. This method shows better robustness against load variation and shorter fault detection time (a quarter of the electrical period). However, its effectiveness has not been verified during motor acceleration/deceleration, and its robustness against parameter variation is unknown.

Through the published fault diagnosis methods, it can be noticed that the robustness and rapidity are hard to balance for the conventional fault diagnosis method, particularly in the variable speed condition. Therefore, further studies are still necessary.

This article proposes a novel switch open-fault diagnosis method based on the differential current observer. Owing to the differential operation for motor three-phase currents, the designed observer shows superior anti-interference ability, and the fault can be diagnosed by simple residuals processing and FDI logics. To further improve its robustness under different operating conditions, an adaptive fault detection threshold is designed. As a result, superior robustness against speed change, load variation, and parameter errors can be obtained, with fast detection speed. The rest of this article is organized as follows. The terminal voltage distortions induced by switch open fault are analyzed in Section II. A new differential current observer-based fault diagnosis method with an adaptive threshold is proposed in Section III. Sufficient experiments are developed in Section IV. Finally, Section V concludes this article.

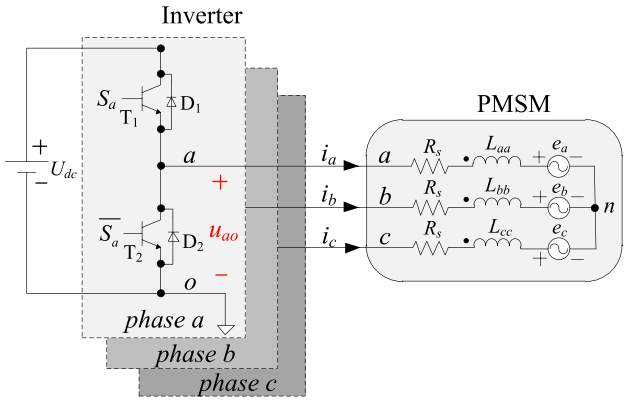

Fig. 1. Three-phase VSI-based PMSM drive system.

II. Terminal Voltage Distortions Induced by Switch Open Fault

Switch open fault in VSI leads to voltage distortions in PMSM, which can be utilized to diagnose the fault. Hence, the motor voltages change laws under faulty conditions are analyzed.

A. Terminal Voltage Expression Under Faulty Condition

The typical three-phase VSI-based PMSM drive system can be described in Fig. 1. The PMSM three-phase voltage equation under healthy condition can be written as

$$\begin{bmatrix} u_{an} \\ u_{bn} \\ u_{cn} \end{bmatrix} = \begin{bmatrix} R_s & 0 & 0 \\ 0 & R_s & 0 \\ 0 & 0 & R_s \end{bmatrix} \begin{bmatrix} i_a \\ i_b \\ i_c \end{bmatrix} + \begin{bmatrix} L_{aa} & M_{ab} & M_{ac} \\ M_{ab} & L_{bb} & M_{bc} \\ M_{ac} & M_{bc} & L_{cc} \end{bmatrix} \frac{d}{dt} \begin{bmatrix} i_a \\ i_b \\ i_c \end{bmatrix} + \begin{bmatrix} e_a \\ e_b \\ e_c \end{bmatrix} \quad (1)$$

where u_{an}, u_{bn}, and u_{cn} are the three-phase voltages, i_a, i_b, and i_c are the three-phase currents, e_a, e_b, and e_c are the three-phase back electromotive forces (EMFs), R_s is the phase resistance, L_{aa}, L_{bb}, and L_{cc} are the three-phase self-inductances, and M_{ab}, M_{ac}, and M_{bc} are the phase mutual inductances.

Assuming that PMSM is three-phase symmetrical, i.e., $L_{aa} = L_{bb} = L_{cc} = L$, $M_{ab} = M_{bc} = M_{ac} = M$, (1) can be

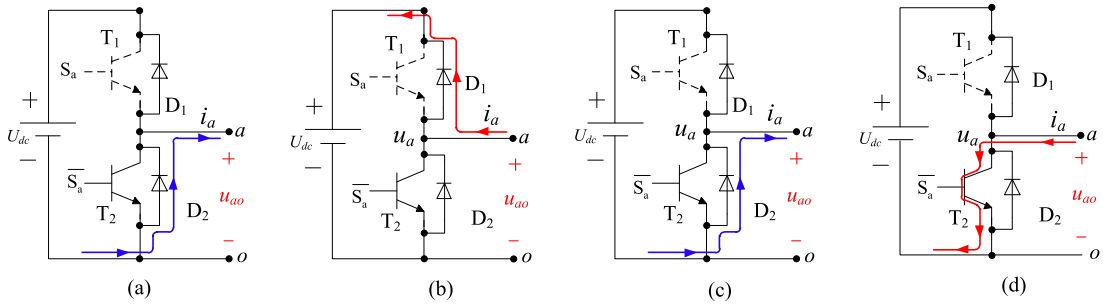

Fig. 2. Current paths of i_a under switch T_1 open fault. (a) $S_a = 1$ and $i_a > 0$. (b) $S_a = 1$ and $i_a < 0$. (c) $S_a = 0$ and $i_a > 0$. (d) $S_a = 0$ and $i_a < 0$.

TABLE I
INSTANT TERMINAL VOLTAGE UNDER SWITCH T_1 OPEN FAULT

Switching Signal	i_a>0	i_a<0
S_a=0	u_{ao}=0	u_{ao} =0
S_a=1	u_{ao} =0	u_{ao}=U_{dc}

simplified as

$$u_{xn} = R_s i_x + (L - M)\frac{di_x}{dt} + e_x \tag{2}$$

where u_{xn}, i_x, and e_x are, respectively, the phase voltage, current, and back EMF of phase x, and $x = a, b, c$.

Normally, through controlling the switching signal, the motor terminal voltage is clamped close to zero or $U_{\rm dc}$

$$u_{xo} = S_x \cdot U_{\rm dc}, i_x \neq 0 \tag{3}$$

where u_{xo} is the terminal voltage with respect to ground (negative end of dc bus) of phase x, U_{dc} is the dc bus voltage, and S_x is the switch signal.

Through conducting state-space averaging operation for u_{xo}, the average terminal voltage ($\bar{u}_{xo}$) can be derived as

$$\bar{u}_{xo} = u^*_{xo}, i_x \neq 0 \tag{4}$$

where u^*_{xo} is the terminal voltage command given by current loop and $u^*_{xo} = d_x \cdot U_{dc}$, and d_x is the duty cycle of S_x.

In order to illustrate the current and voltage variations induced by fault, switch T_1 open fault is taking as an example here. After switch T_1 opens, the paths of phase current i_a can be described in Fig. 2. It can be seen that when $S_a = 1$ and $i_a > 0$, i_a would freewheeling through diode D_2 and u_{ao} is clamped to zero [see Fig. 2(a)]. Similarly, the current paths under other conditions can be described as Fig. 2(b)–(d), and the values of u_{ao} can be obtained as given in Table I.

In the case of $i_a = 0$, phase A can be regarded as disconnected from the bridge arm. Thus, its terminal voltage u_{ao} is not controlled by the switching signal S_a. To calculate u_{ao} under such condition, PMSM three-phase voltage equation [see (2)] is utilized. By substituting $i_a = 0$ into (2) and ignoring the inductance term, it can be derived that phase voltage u_{an} equals phase back EMF, i.e., $u_{an} = e_a$.

According to [28], the relationship between motor terminal voltages and phase voltages can be expressed as

$$u_{an} = (2u_{ao} - u_{bo} - u_{co})/3. \tag{5}$$

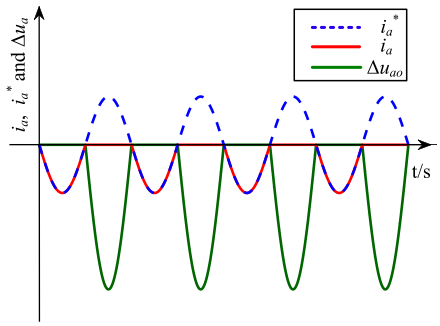

Fig. 3. Phase current and terminal voltage distortion after switch T_1 open fault.

Substituting $u_{an} = e_a$ into (5), the terminal voltage u_{ao} can be derived as

$$u_{ao} = \frac{1}{2} \cdot (3e_a + u_{bo} + u_{co}), i_a = 0. \tag{6}$$

From Table I and (6), the postfault average terminal voltage $\bar{u}_{ao}$ can be obtained as

$$\bar{u}_{ao} = \begin{cases} u^*_{ao}, & i_a < 0 \\ \frac{1}{2} \cdot (3e_a + u^*_{bo} + u^*_{co}), & i_a = 0 \\ 0, & i_a > 0. \end{cases} \tag{7}$$

Noticed that after switch T_1 open fault, the average terminal voltage $\bar{u}_{ao}$ equals its reference only when $i_a < 0$. Therefore, the system can be considered as healthy when $i_a < 0$, but it must be regarded as faulty under other conditions.

B. Terminal Voltage Distortion Characteristics After Fault

From (7) it can be found that the terminal voltage distortion exists only when $i_a \geq 0$. In order to diagnose the fault correctly, the terminal voltage distortion characteristics should be analyzed. Assuming that phase current reference $i^*_a > 0$, then i_a would try to track its reference. However, according to Table I and (7), the terminal voltage u_{an} is negative when $i_a > 0$, which leads to a continued decline in i_a until i_a is no longer positive. Thus, i_a cannot be positive stably. Instead, it will be near zero as shown in Fig. 3 [31]. Therefore, terminal voltage distortion should be considered only when i_a is near zero.

TABLE II
POLARITIES OF TERMINAL VOLTAGE DISTORTIONS UNDER DIFFERENT FAULT SOURCES

Faulty switch	Voltage Distortions	Polarities	Conditions for nonzero distortion
T_1	Δu_{ao}	-	$i_a^* > 0$
T_2	Δu_{ao}	+	$i_a^* < 0$
T_3	Δu_{bo}	-	$i_b^* > 0$
T_4	Δu_{bo}	+	$i_b^* < 0$
T_5	Δu_{co}	-	$i_c^* > 0$
T_6	Δu_{co}	+	$i_c^* < 0$

From (7), the terminal voltage distortion induced by the fault can be derived as

$$\Delta u_{ao} = \bar{u}_{ao} - u^*_{ao} = \begin{cases} \frac{3e_a + u^*_{bo} + u^*_{co} - 2u^*_{ao}}{2}, & i_a \approx 0 \\ 0, & i_a < 0 \end{cases} \quad (8)$$

where Δu_{ao} is the fault-induced terminal voltage distortion.

As for the three-phase PMSM, its voltage references satisfy the following equation:

$$\begin{aligned} u^*_{an} + u^*_{bn} + u^*_{cn} &= 0 \\ u^*_{xn} - u^*_{yn} &= u^*_{xo} - u^*_{yo} \end{aligned} \quad (9)$$

where u^*_{an}, u^*_{bn}, and u^*_{cn} are the motor phase voltage references, u^*_{xn} and u^*_{yn} are the phase voltage references of phases x and y, respectively, and u^*_{xo} and u^*_{yo} are the corresponding terminal voltage commands.

Substituting (9) into (8), the terminal voltage distortion can also be expressed as

$$\Delta u_{ao} = \begin{cases} -\frac{3(u^*_{an} - e_a)}{2}, & i_a = 0 \\ 0, & i_a < 0. \end{cases} \quad (10)$$

In (10), $(u^*_{an} - e_a)$ can be regarded as the expected voltage drop on inductance and resistance of phase A according to (2). Thus, it can be approximated as

$$u^*_{an} - e_a = R_s i^*_a + (L - M)\frac{di^*_a}{dt}. \quad (11)$$

Ignoring the phase lag caused by the inductance term in (11), $(u^*_{an} - e_a)$ is proportional to i^*_a. Therefore, the terminal voltage distortion $\triangle u_{ao}$ in (10) varies with i^*_a after switch T_1 open fault, as shown in Fig. 3. Consequently, the polarities of terminal voltage distortions under different open-switch faults can be obtained, as given in Table II.

From the last column of Table II, it can be noted that the VSI works abnormally only under certain conditions. For simplicity, the following analysis only refers to the section that voltage distortion is nonzero.

III. DIFFERENTIAL CURRENTS OBSERVER-BASED FAULT DIAGNOSIS METHOD

The terminal voltage/current distortions caused by the switch open fault can be monitored by voltage/current state observers. To achieve superior fault diagnosis performance, a new differential current observer-based fault diagnosis method is proposed in this article. Especially, the fault detection threshold is adaptive regulated.

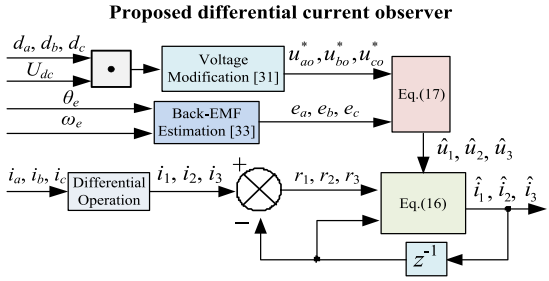

Fig. 4. Diagram of the proposed differential current observer.

A. Differential Current Observer

Based on (2), PMSM current state equation can be derived as

$$\frac{di_x}{dt} = -\frac{R_s}{L - M} \cdot i_x + \frac{1}{L - M} \cdot (u_{xn} - e_x). \quad (12)$$

Then, the discrete phase current state equation can be obtained as

$$i_x(k+1) = g \cdot i_x(k) + h \cdot (u_{xn}(k) - e_x(k)) \quad (13)$$

where coefficients $g = \exp\{-R_s T_s/(L-M)\}$ and $h = (1-g)/R_s$, and T_s is current sampling time.

Thus, the phase current observer can be designed as

$$\hat{i}_x(k+1) = g \cdot \hat{i}_x(k) + h \cdot (u_{xn}(k) - e_x(k)) \quad (14)$$

where $\hat{i}_x$ is the estimated phase current and k is the iteration integer.

Considering that the circuit noise would degrade the observer performance, a new closed-loop differential current observer is proposed in this article. It can be written as

$$\hat{i}_j(k+1) = g \cdot \hat{i}_j(k) + h \cdot \hat{u}_j(k) + l_j \cdot (i_j(k) - \hat{i}_j(k)) \quad (15)$$

where $j = 1, 2, 3$, i_j is the actual differential current, $[i_1, i_2, i_3] = [i_a - i_b, i_b - i_c, i_c - i_a]$, $\hat{i}_j$ is the estimated differential current, the difference between i_j and $\hat{i}_j$ is defined as residual r_j for short, l_j is the feedback coefficient, and $\hat{u}_j$ is the estimated equivalent input, which can be calculated as

$$\begin{bmatrix} \hat{u}_1(k) \\ \hat{u}_2(k) \\ \hat{u}_3(k) \end{bmatrix} = \begin{bmatrix} u^*_{an}(k) - u^*_{bn}(k) - e_a(k) + e_b(k) \\ u^*_{bn}(k) - u^*_{cn}(k) - e_b(k) + e_c(k) \\ u^*_{cn}(k) - u^*_{an}(k) - e_c(k) + e_a(k) \end{bmatrix}. \quad (16)$$

Substituting (9) into (16), the estimated equivalent input can be written as

$$\begin{bmatrix} \hat{u}_1(k) \\ \hat{u}_2(k) \\ \hat{u}_3(k) \end{bmatrix} = \begin{bmatrix} u^*_{ao}(k) - u^*_{bo}(k) - e_a(k) + e_b(k) \\ u^*_{bo}(k) - u^*_{co}(k) - e_b(k) + e_c(k) \\ u^*_{co}(k) - u^*_{ao}(k) - e_c(k) + e_a(k) \end{bmatrix}. \quad (17)$$

The back EMF e_x in (17) can be estimated with electrical speed ω_e, electrical angel θ_e, and the back EMF waveform functions [32].

The diagram of the proposed observer can be described as Fig. 4. For the closed-loop observer, its performance heavily

depends on the feedback coefficient. Generally, the observer closed-loop pole is expected to be 3–5× faster than the current loop pole. Therefore, the feedback coefficient can be determined according to the expected pole of the observer. Considering that the PMSM is approximately three-phase symmetrical, the three feedback coefficients can be selected equal ($l_1 = l_2 = l_3 = l$) for simplicity.

Through differential operation and closed-loop design, the anti-interference of the observer can be improved distinctly, and accurate residuals can be obtained.

B. Residual Characteristics Analysis

Terminal voltage distortion leads to differential current deviations (residuals). Therefore, the residual characteristics are analyzed for fault diagnosis rule making.

By conducting differential operation for (13), the motor differential current state equation can be written as

$$i_j(k+1) = g \cdot i_j(k) + h \cdot u_j(k) \tag{18}$$

where u_j is the actual equivalent input, $u_j = u_j^* + \Delta u_j$, Δu_j is the differential voltage deviations induced by switch open fault, $\Delta u_1 = \Delta u_a - \Delta u_b$, $\Delta u_2 = \Delta u_b - \Delta u_c$, and $\Delta u_3 = \Delta u_c - \Delta u_a$.

Subtracting (15) from (18), the residual state equation can be obtained as

$$r_j(k+1) = (g-l) \cdot r_j(k) + h \cdot \Delta u_j(k). \tag{19}$$

Conducting z-transform for (19), the transfer function from voltage distortion to residual can be derived as

$$G_j(z) = \frac{R_j(z)}{\Delta U_j(z)} = \frac{h}{z - z_p} \tag{20}$$

where $R_j(z)$ and $\Delta U_j(z)$ are the z-transforms of r_j and Δu_j, respectively, and z_p is the pole of the observer, $z_p = g - l$.

From (20), it can be seen that $G_j(z)$ is a first-order inertial element. Therefore, r_j is determined by Δu_j (terminal voltage distortion essentially) with short inertia delay.

In healthy conditions, the terminal voltage distortions are very small, thus the induced residuals can be neglected. Once the switch open fault appears, the subsequent voltage distortions would lead to nonzero residuals.

To analyze the residual characteristics conveniently, defining residual vector as $\boldsymbol{r} = [r_1, r_2, r_3]^{\mathrm{T}}$, and its normalized vector as $\boldsymbol{r_n} = \boldsymbol{r}/\|\boldsymbol{r}\|_2$ ($\|\bullet\|_2$ is the modular operation). According to Table II, it can be seen that when switch T_1 is open, $\Delta u_{ao} < 0$ and $\Delta u_{bo} = \Delta u_{co} = 0$. Thus, $\Delta u_1 = -\Delta u_3 < 0$, $\Delta u_2 = 0$. Then, the induced residuals satisfy $r_1 = -r_3 < 0$, $r_2 = 0$ as well. Thus, it can be derived that the normalized residual vector $\boldsymbol{r_n}^{\mathrm{T}} = [-1, 0, 1]/\sqrt{2}$ is fixed. Similarly, the normalized residual vector under other open-switch faults can be calculated, as given in Table III.

It can be noticed that the open-switch fault leads to a nonzero and direction-fixed residual vector, which can be adopted for fault detection and isolation.

TABLE III
NORMALIZED RESIDUAL VECTORS UNDER FAULT CONDITIONS

Fault Source	Voltage Distortions	$\boldsymbol{r_n}^{\mathrm{T}}$
T_1	Δu_1=-Δu_3<0	$\boldsymbol{r_{n1}}^{\mathrm{T}}$=(-1,0,1)/√2
T_2	Δu_1=-Δu_3>0	$\boldsymbol{r_{n2}}^{\mathrm{T}}$=(1,0,-1)/√2
T_3	Δu_1=-Δu_2>0	$\boldsymbol{r_{n3}}^{\mathrm{T}}$=(1,-1,0)/√2
T_4	Δu_1=-Δu_2<0	$\boldsymbol{r_{n4}}^{\mathrm{T}}$=(-1,1,0)/√2
T_5	Δu_2=-Δu_3<0	$\boldsymbol{r_{n5}}^{\mathrm{T}}$=(0,-1,1)/√2
T_6	Δu_2=-Δu_3>0	$\boldsymbol{r_{n6}}^{\mathrm{T}}$=(0,1,-1)/√2

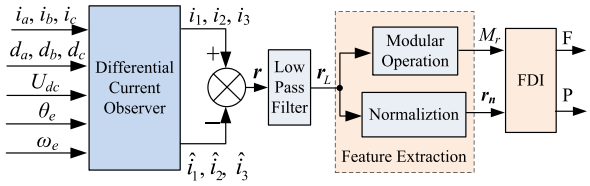

Fig. 5. Diagram of the proposed fault diagnosis method.

C. Proposed Fault Diagnosis Method

The proposed fault diagnosis method diagram can be described as Fig. 5. It mainly includes four modules, differential currents observer, low-pass filter, feature extraction module, and FDI module. First, the actual differential currents and their estimated values are calculated with the differential current state observer (see Fig. 4). By comparing the actual differential currents with their estimated values, the residual vector $\boldsymbol{r}$ is obtained, which is then put into the low-pass filter to reduce noise. Through the modular and normalization operation for the filtered residual vector, diagnostic variables (M_r and $\boldsymbol{r_n}$) can be obtained and employed for FDI.

In the FDI module, the fault detection logic is defined as

$$\mathrm{F} = (\mathrm{sign}(M_r - T_h) + 1)/2 \tag{21}$$

where F is the fault status variable (F = 0 switch healthy, while F = 1 switch fault), M_r is the modulus of the residual vector, and T_h is the fault detection threshold.

As for the fault isolation, it is achieved based on minimal-distance principle as

$$\|\boldsymbol{r_n} \boldsymbol{r_{n\mathrm{P}}}\|_2 = \min_{k=16} (\|\boldsymbol{r_n} \boldsymbol{r_{nk}}\|_2) \tag{22}$$

where $\boldsymbol{r_{nk}}$ represents the ideal normalized residual vector listed in Table III, k = 1–6, subscript P is the fault source indicator ($\mathrm{T_P}$ is the faulty switch), and $\|\bullet\|_2$ is the modular operation, respectively.

The low-pass filter in Fig. 5 is a first-order inertial element. To balance the filtering delay and filtering performance, the cutoff frequency of the filter can be set as 1/15–1/30 of the voltage PWM frequency.

D. Adaptive Threshold for Fault Detection

Considering that interferences and model errors may degrade observer accuracy and lead to false/missed detection

subsequently, an adaptive fault detection threshold is designed in this article.

Taking the model errors into account, the differential current state equation [see (18)] can be written as

$$\boldsymbol{i}(k+1) = G' \cdot \boldsymbol{i}(k) + H' \cdot (\hat{\boldsymbol{u}}(k) + \boldsymbol{u_f}(k)) \tag{23}$$

where G' and H' are the actual state transition matrix and control matrix, respectively, $\boldsymbol{i}$ is the differential current vector, $\boldsymbol{i} = [i_1, i_2, i_3]^{\mathrm{T}}$, $\hat{\boldsymbol{u}}$ is the estimated equivalent input vector, $\hat{\boldsymbol{u}} = [\hat{u}_1, \hat{u}_2, \hat{u}_3]^{\mathrm{T}}$, $\boldsymbol{u_f}$ is the differential voltage distortion vector, and $\boldsymbol{u_f} = [\Delta u_1, \Delta u_2, \Delta u_3]^{\mathrm{T}}$.

By subtracting (15) from (23), the residual state equation can be obtained as

$$\boldsymbol{r}(k+1) = z_p \cdot \boldsymbol{r}(k) + \Delta G \cdot \boldsymbol{i}(k) + \Delta H \cdot \hat{\boldsymbol{u}}(k) + H' \cdot \boldsymbol{u_f}(k) \tag{24}$$

where $\Delta G = G' - g \cdot E$, $\Delta H = H' - h \cdot E$, and E is the unit matrix.

The z-transform of (24) can be derived as

$$\boldsymbol{R}(z) = M_i(z) \cdot \boldsymbol{I}(z) + M_u(z) \cdot \boldsymbol{U}^*(z) + M_f(z) \cdot \boldsymbol{U_f}(z) \tag{25}$$

where $\boldsymbol{R}$(z), $\boldsymbol{I}$(z), $\hat{\boldsymbol{U}}(z)$, and $\boldsymbol{U_f}$(z) are the z-transforms of variables $\boldsymbol{r}$, $\boldsymbol{i}$, $\hat{\boldsymbol{u}}$, and $\boldsymbol{u_f}$, respectively, $M_i = \Delta G/(z - z_{\mathrm{p}})$, $M_u = \Delta H/(z - z_{\mathrm{p}})$, and $M_f = H'/(z - z_{\mathrm{p}})$.

From (25), it can be seen that the residual vector relates to $\boldsymbol{i}$ and $\hat{\boldsymbol{u}}$, thus it varies with motor operating conditions as well. If the fault detection threshold is set a fixed value as in the conventional method, false/missed detection may occur once the load or motor speed changes. To diagnose fault correctly, threshold T_h is expected to be larger than M_r in healthy condition but smaller after the fault. Therefore, the upper bound of M_r in normal condition should be analyzed first.

It is found that the transfer functions M_i and M_u can be regarded as inertial elements. From (25), it can be derived that in healthy condition, if the phase lags caused by inertial elements are neglected, the residual satisfies

$$M_r < m_1 \cdot ||\boldsymbol{i}||_2 + m_2 \cdot ||\hat{\boldsymbol{u}}||_2 \tag{26}$$

where $m_1 = (1\text{-}z_{\mathrm{p}})^{-1} \cdot \mathrm{sum}(|\Delta G|)$, $m_2 = (1 - z_{\mathrm{p}})^{-1} \cdot \mathrm{sum}(|\Delta H|)$, $|\cdot|$ is the absolute value symbol, and sum(·) is the function to add up all elements of a matrix.

With the derived upper bound, the threshold T_h can be designed as

$$T_{h1} = T_0 + m_1 \cdot ||\boldsymbol{i}||_2 + m_2 \cdot ||\hat{\boldsymbol{u}}||_2 \tag{27}$$

where T_0 is a small positive constant.

It should be noticed that phase lags are ignored in the derivation of (26). But T_{h1} should be synchronized with M_r to avoid false detection caused by the phase lags. The signal synchronization method is shown in Fig. 6, where the inertial element I_e(z) is inserted to compensate the phase lag 1, and the bottom two filters are designed the same as the top one to compensate the phase lag 2.

To fully compensate the phase lag 1, the inertial element is designed as

$$I_e(z) = \frac{1 - z_p}{z - z_p}. \tag{28}$$

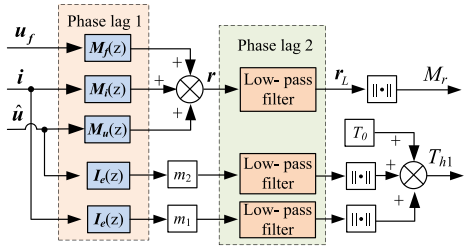

Fig. 6. Synchronization for fault detection threshold and index.

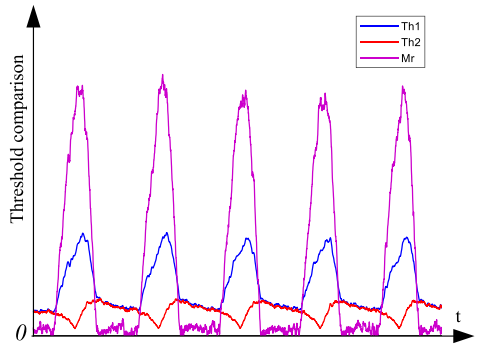

Fig. 7. Waveforms of the two adaptive thresholds.

With the adaptive threshold T_{h1}, false detection can be avoided. However, a high missed detection rate would be induced, especially under light load (illustration is shown in the Appendix). To reduce missed detection, the threshold T_h should be redesigned.

From (23), it can be found that in healthy condition ($\boldsymbol{u_f} = \boldsymbol{0}$), $\hat{\boldsymbol{u}}$ can be calculated as

$$\hat{\boldsymbol{u}}(k) = (H')^{-1} \cdot (\boldsymbol{i}(k+1) - G' \cdot \boldsymbol{i}(k)) \approx \frac{1}{h}(\boldsymbol{i}(k+1) - \boldsymbol{i}(k)) \tag{29}$$

in which the approximate conditions are $H' \approx H = h$E, G' $\approx G = g$E, $g = \exp\{-R_s \mathrm{T_s}/(L-M)\} \approx 1$.

Substituting (29) into (27), a new adaptive threshold can be obtained

$$T_{h2} = T_0 + m_1 \cdot ||\boldsymbol{i}||_2 + m_3 \cdot ||\Delta \boldsymbol{i}||_2 \tag{30}$$

where $\Delta \boldsymbol{i}$(k) = $\Delta \boldsymbol{i}$(k + 1) − $\boldsymbol{i}$(k), $m_3 = m_2$/h, respectively. Note that the selection of parameters m_1 and m_3 in (30) heavily relies on model errors (ΔG and ΔH), which are unavailable normally. In practice, ΔG and ΔH can therefore be roughly set as large values (estimated when resistance and inductance vary 30% and 50%, respectively). As for T_0, it can be roughly set to 10% of the motor rated current and then fine-tuned under no-load condition.

Noticed that T_{h1} and T_{h2} are almost equal under healthy conditions, false detection can be therefore avoided. Under faulty conditions, $\|\boldsymbol{i}\|$ and $\|\Delta \boldsymbol{i}\|_2$ decrease (see the Appendix), which leads to a decline in adaptive threshold T_{h2} after the fault (see Fig. 7). As a result, the missed detection rate as well as the detection time can be reduced. Consequently, the robustness of the fault diagnosis method can be improved significantly through the designed adaptive threshold, without sacrificing the rapidity.

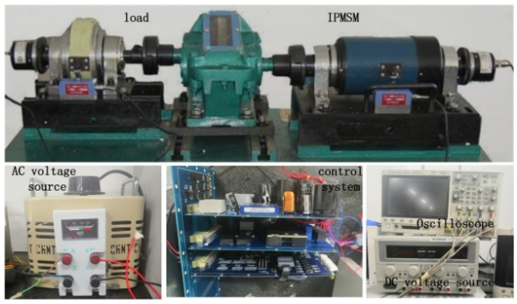

Fig. 8. PMSM experimental platform.

TABLE IV
PARAMETERS OF THE PMSM CONTROL SYSTEM

Parameters	Unit	Value
Rated Power	W	120
Rated Current	A	3.1
Rated Output Torque	N·m	1.1
Rated Rotor Speed	rpm	1000
Flux Linkage	Wb	0.13
Phase Resistance	Ω	0.67
Phase Inductance	mH	3.4
Mutual Inductance	mH	-1.6
Pole Pairs	—	2
DC Bus Voltage	V	50
PWM Frequency	kHz	20
Current Sampling Time	s	5×10^{-5}
Angle Sampling Time	s	6.5×10^{-4}

IV. PMSM CONTROL SYSTEM EXPERIMENT

A. Experimental Setup

Sufficient experiments have been performed on the three-phase PMSM plat shown in Fig. 8. The digital signal processor (DSP TMS320F28335) based PMSM control system is used for the experiment. Rotor position is measured with a 12-bit absolute encoder. Hall current sensors are used to measure the phase currents of the PMSM. The inverter circuit includes an integrated power module, which is powered by the dc voltage source. The motor load is provided by a magnetic powder brake. The main parameters of the system are listed in Table IV.

In tests, the feedback gain l, threshold coefficients T_0, m_1, and m_3 are selected as $l = 0.20$, $T_0 = 0.3$, $m_1 = 0.2$, and $m_3 = 4$. The open-switch fault is simulated by removing the gate signal of the "faulty" transistor. In this article, the proposed open-phase fault diagnosis method is compared with the method in [30]. Based on these settings, detailed experiments are performed.

B. Experiment I: Effectiveness and Rapidity Comparison in Variable-Speed System

First, the effectiveness of the proposed fault diagnosis method is verified at the rated condition. The motor operates at rated speed (1000 r/min) under rated load (1.1 N·m). Both the upper switch (T_1) and bottom switch (T_2) open faults are simulated to verify the effectiveness. Switch T_1 opens at $t = 0.105$ s in the first test, while the switch T_2 open fault occurs at $t = 0.100$ s in the second test. The experimental results of the proposed method are shown in Figs. 9 and 10.

From Fig. 9, it can be seen that before the fault, the motor operates smoothly, and the fault detection index M_r is far below the threshold T_{h2}. However, the switch open fault leads to serving distortions in motor three-phase currents, thus induces great fluctuations in d–q currents and motor speed (see Fig. 9(a)–(c)]. Meanwhile, from Fig. 9(e), it can be observed that once the switch open fault occurs, T_{h2} does decrease significantly, and the rising index M_r exceeds the falling threshold T_{h2} quickly. It contributes to a fast fault detection speed (within 2.9 ms, 9.7% of a current period) and a lower missed detection rate. Moreover, the residuals waveforms [see Fig. 9(d)] show that the normalized residual vector is near to $\boldsymbol{r_{n1}}^{\mathrm{T}} = (-1, 0, 1)/\sqrt{2}$, which is consistent with Table III. Consequently, the fault is detected and located successfully, as shown in Fig. 9(f). From Fig. 10, it can be found that the fault occurs at the lower switch of the inverter leg can also be detected and located with the proposed method, which proves that the effectiveness of the method is independent of the fault source.

Second, the proposed method is tested during motor acceleration and deceleration under rated load. In the acceleration test, switch T_1 open fault occurs at $t = 0.17$ s, during motor acceleration from 500 to 1000 r/min. As for the deceleration test, the fault happens at $t = 0.13$ s, during motor deceleration from 1000 to 250 r/min.

From Fig. 11(a)–(d), it can be seen that the switch open fault leads to motor speed fluctuation no matter the motor is accelerating or decelerating. It can be noted that the threshold T_{h2} is higher than index M_r in healthy condition but lower than M_r in faulty condition [see Fig. 11(b) and (e)]. Thus, the proposed method can detect the open switch fault correctly under different motor operating conditions. The diagnostic results, shown in Fig. 11(c) and (f), indicate correct fault detection and localization. The above experiment results verify the effectiveness of the proposed fault diagnosis method in a variable speed system.

Third, the rapidity of the proposed fault diagnosis method is verified and compared with that of the conventional method [30]. The corresponding experiment results are described in Fig. 12. Here, T_a and R_a are, respectively, the fault detection threshold and index in the conventional method, while F_1 and F_2 are the fault detection results of the proposed method and conventional method, respectively.

From Fig. 12(a) and (b), it can be seen that the fault detection indexes (M_r and R_a) increase rapidly after the fault both in the proposed method and in the conventional method. But the adaptive threshold T_a rises while T_{h2} falls after the fault occurrence. As a result, much faster fault detection speed can be achieved by the proposed method in all of the three tests [see Fig. 12(c)]. For quantitative comparison, the fault detection times of these two methods are listed in Table V. The proposed method shows superior rapidity compared with the conventional method.

It can be noticed that the fault detection times of the proposed method are quite different in the three tests. Actually, the fault detection time for the proposed method mainly includes two parts. One is the time delay caused by data processing links

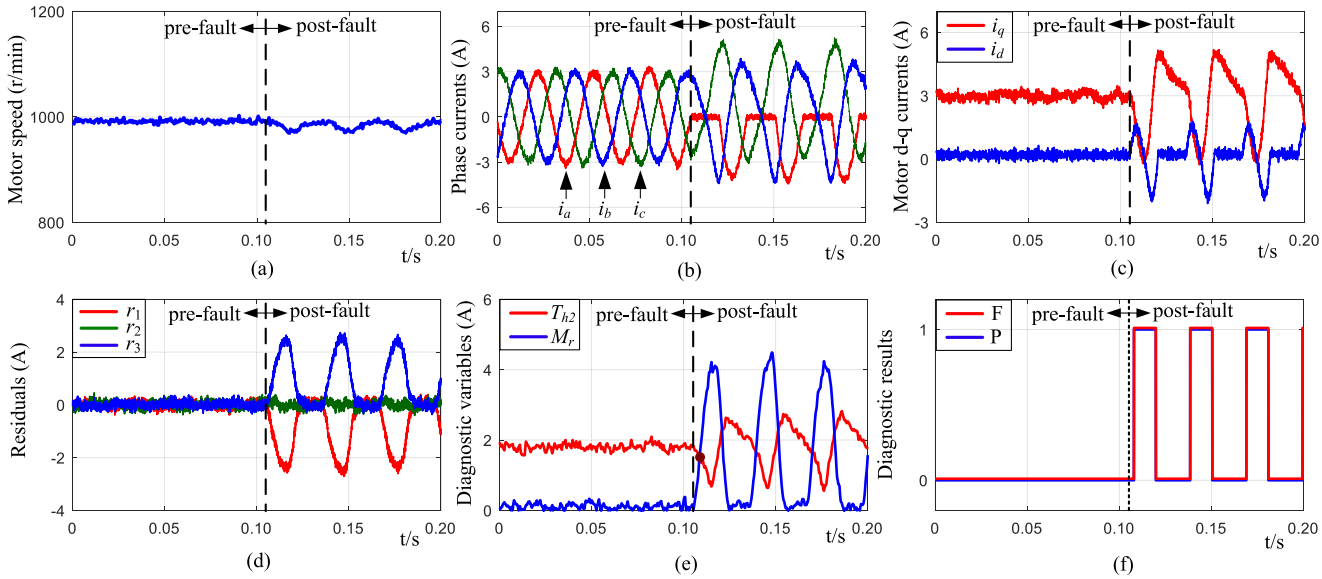

Fig. 9. Effectiveness test of the proposed method at rated speed. (a) Motor speed. (b) Motor three-phase currents. (c) Motor *d*–*q* currents. (d) Residual components. (e) Fault diagnostic variables. (f) Fault diagnostic results.

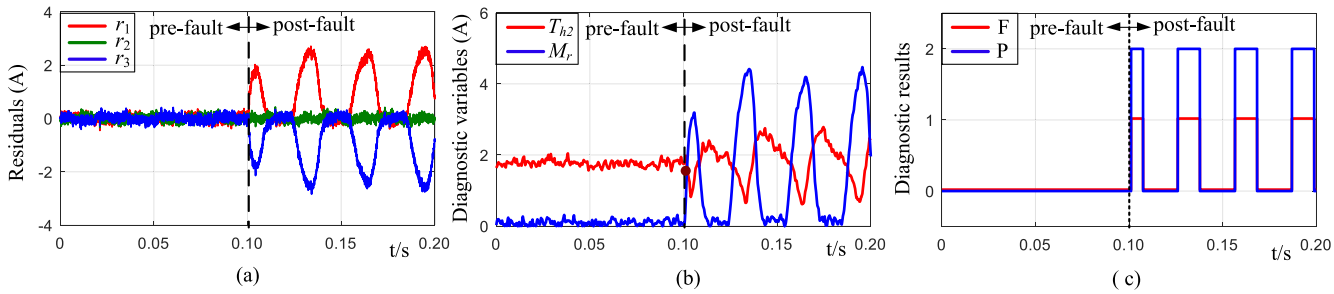

Fig. 10. Detection of the open-switch fault on T_2. (a) Residual components. (b) Diagnostic variables. (c) Diagnostic results.

TABLE V
FAULT DETECTION TIMES IN EXPERIMENT I

Methods	Rated-speed	Acceleration	Deceleration
Proposed method	2.9ms	1.2ms	1.3ms
Conventional method	6.5ms	4.1ms	9.0ms

(such as the observer and low pass filter), which varies with observer closed-loop pole and filter cutoff frequency. And the other one is the time required for voltage distortion to become large enough (to make the index M_r larger than threshold T_{h2}). As the voltage distortion is approximate the periodic function of the electrical angle (see Fig. 3), the second part relates to the electrical angle at fault occurrence. In the three tests, the electrical angles at fault occurrence are different, which leads to different fault detection times.

C. Experiment II: Robustness Against Load Variation

In this experiment, the robustness of the proposed method against load variation is verified under healthy and faulty conditions respectively.

First, the comparative test between the proposed method and the conventional method is conducted under healthy conditions. In the test, the motor operates at rated speed, and the load torque changes from the light load (0.11 N·m) to rated load (1.1 N·m) at $t = 0.15$ s and the corresponding experimental results are reported in Fig. 13. From Fig. 13(a), it can be found that the index R_a is larger than the threshold T_a under light load in the conventional method. This eventually leads to false detection. Thus, the fault detection result of the conventional method is unreliable under the light load conditions. Under the same condition, the comparative test with the proposed method is developed, as described in Fig. 13(b). It can be seen that the index M_r in the proposed method is always below the threshold T_{h2}. Therefore, false detection would not appear with the proposed method under healthy conditions, even when the load mutates from light value to rated value. The proposed method possesses superior robustness against load variation than the conventional method.

Second, the robustness of the proposed method is verified under faulty conditions. In this test, switch T_1 open fault occurs at $t = 0.1$ s, while the motor load changes from 0.11 N·m to rated load 1.1 N·m at $t = 0.2$ s. The experimental results are shown

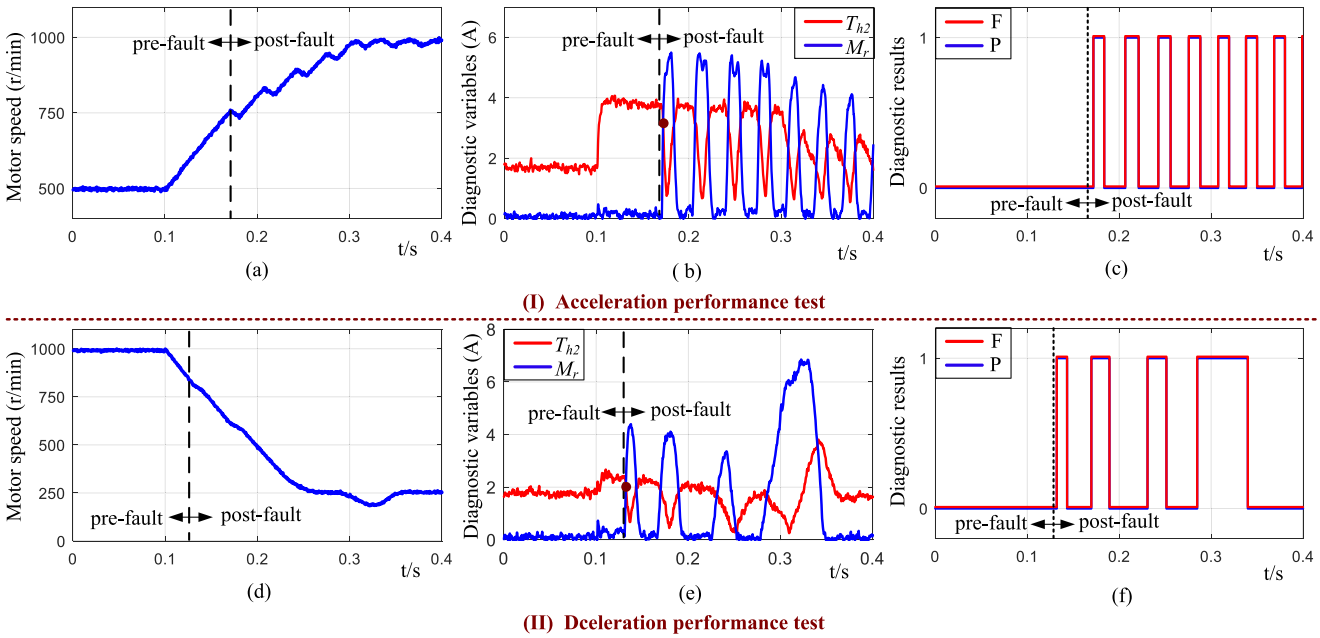

Fig. 11. Effectiveness test of the proposed method during motor acceleration and deceleration. (a) Motor speed. (b) Fault diagnostic variables. (c) Fault diagnostic results. (d) Motor speed. (e) Fault diagnostic variables. (f) Fault diagnostic results.

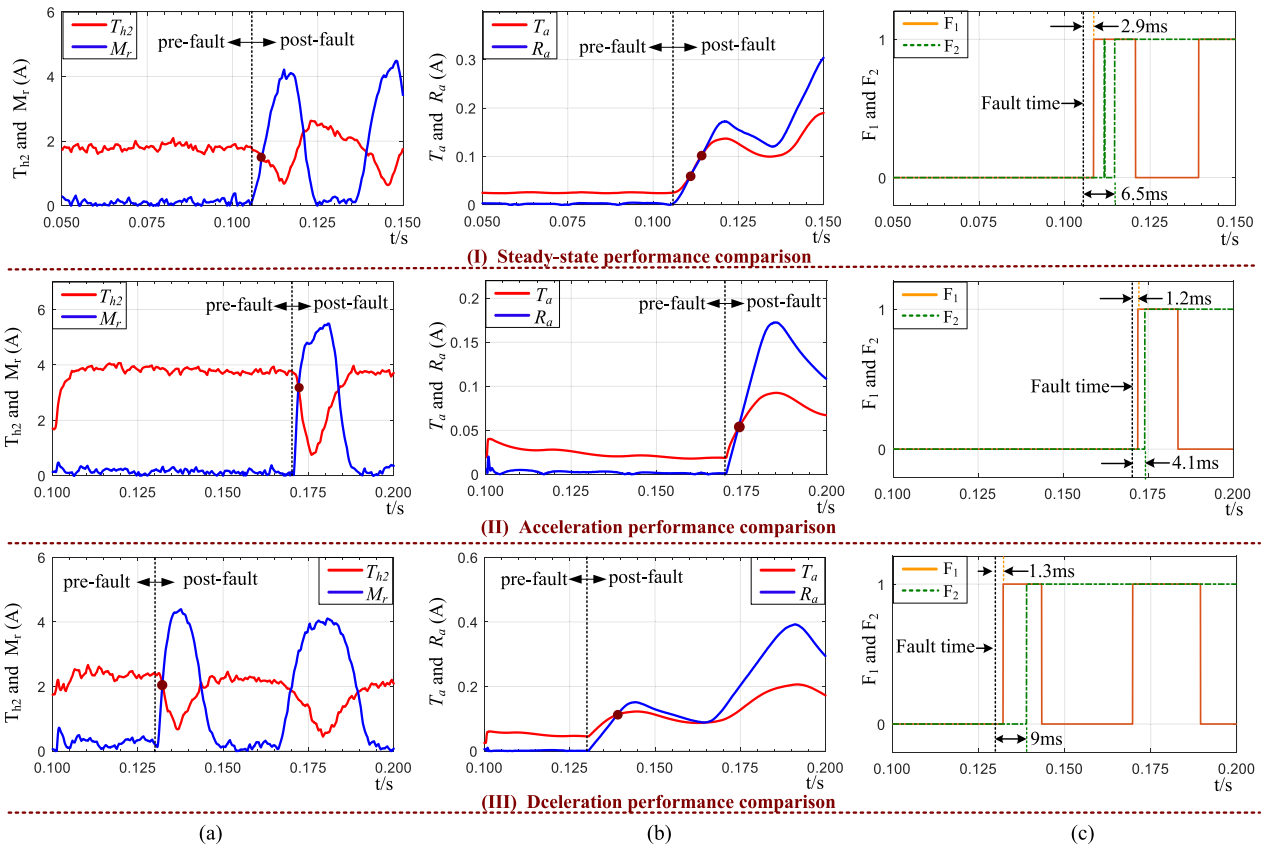

Fig. 12. Rapidity comparison between the two methods. The first and second columns in Fig. 11 are the fault diagnostic variables yielded by the proposed method and conventional method, respectively, and the third column is fault detection result comparison (F_1 and F_2 corresponding to proposed method and conventional method respectively). (a) Diagnostic variables yielded by the proposed method. (b) Diagnostic variables yielded by the conventional method. (c) Fault detection result comparison between the proposed and conventional methods.

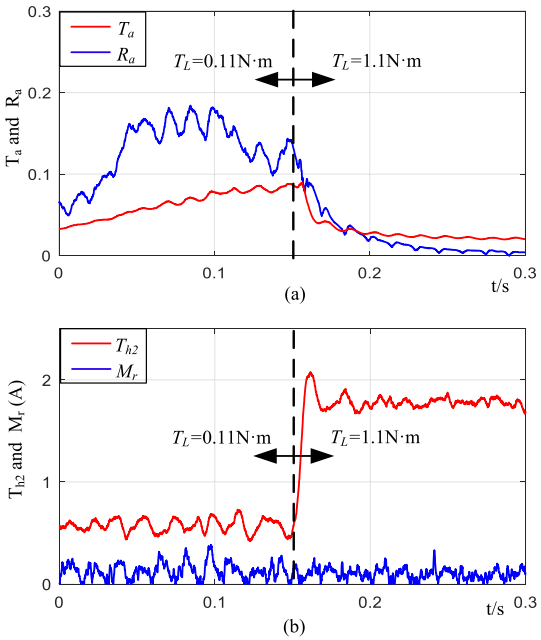

Fig. 13. Robustness comparison with load variation under healthy condition. (a) Response to load variation of the conventional method. (b) Response to load variation of the proposed method.

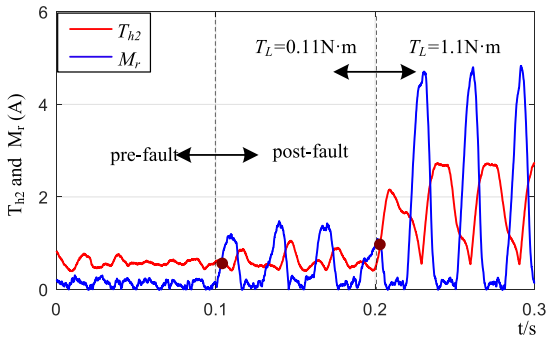

Fig. 14. Responses to load variation under faulty condition.

in Fig. 14. From Fig. 14, it can be seen that M_r is lower than T_{h2} before the fault, but higher than T_{h2} after fault, regardless of the load variation. The results show that load variation would not lead to missed detection in the proposed method.

It should be noticed that in a healthy system, the distance from index M_r to threshold T_{h2} under light load condition is much smaller than under rated load condition [see Fig. 13(b)], and the situation is the same under faulty condition (see Fig. 14). This indicates that the false detection rate and missed detection rate under light load are higher than these under heavy load. Thus, the parameters (such as threshold coefficient T_0 and the filter cutoff frequency) in the proposed method should be finely tuned under a light load.

D. Experiment III: Robustness Against Parameter Variation

In this experiment, the robustness of the proposed method against parameter variation is verified. It is well known that winding resistance and inductance are the key parameters in motor; therefore, two groups' inaccurate values are set for these two parameters in the proposed method during the test. One is

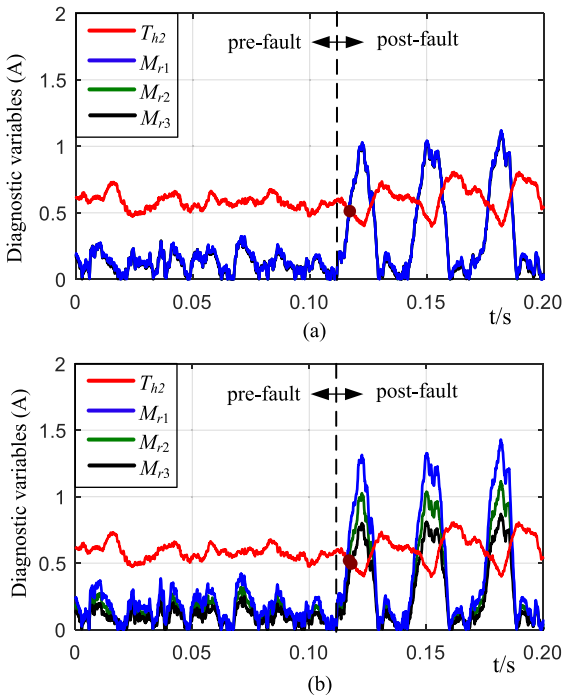

Fig. 15. Robustness test of the proposed method against parameter variations. M_{r0}–M_{r4} are the fault detection indexes under different parameters condition. M_{r0}: $R_s = R_{s0}$ and $L = L_0$; M_{r1}: $R_s = 0.7R_{s0}$ and $L = L_0$; M_{r2}: $R_s = 1.3R_{s0}$ and $L = L_0$; M_{r3}: $R_s = R_{s0}$ and $L = 0.7L_0$; M_{r4}: $R_s = 0.7R_{s0}$ and $L = 1.3L_0$. R_s and L are the observer parameters while R_{s0} and L_0 are motor parameters. (a) Robustness against resistance variations. (b) Robustness against inductance variations.

set as $R_s = R_{s0}$, $R_s = 0.7R_{s0}$, and $R_s = 1.3R_{s0}$, another is set as $L = L_0$, $L = 0.7L_0$, and $L = 1.3L_0$ (R_s, L, and R_{s0}, L_0 are observer and motor parameters, respectively). From the analysis conducted in Section IV-C, it is found that the missed/false detection probability is higher under light load condition. To verify the superiority of the proposed method, the light load (0.11 N·m) is applied in the tests, and the motor operates at 1000 r/min, the switch T_1 open fault occurred at $t = 0.25$ s. With these settings, detailed experiments are conducted. The experimental results are presented in Fig. 15.

From Fig. 15(a), it can be seen that the fault detection indexes (M_{r0}, M_{r1}, and M_{r2}) under different resistance settings almost overlap. It indicates that resistance errors have little effect on the fault detection index. As for the inductance variation, the results are different. From Fig. 15(b), it can be observed that positive inductance error ($L > L_0$) increases the index (M_{r3}). As a result, the false detection rate increases while the missed detection rate decreases. On the contrary, negative inductance error lowers false detection rate but increases missed detection rate. Although the fault detection index changes with the inductance variation, the diagnosis results are correct in all of the tests. The proposed method is robust against parameter variation.

V. Conclusion

This article proposes a novel open switch fault diagnosis method based on the differential current observer. In this method, the residuals are generated from the measured and estimated

differential currents. And the diagnosis variables are obtained by simple feature extraction of the residuals. To avoid false and missed detection caused by the change of operating conditions, an adaptive fault detection threshold is designed. Owing to the self-adjusting characteristics of the designed threshold, superior rapidity and robustness can be obtained, compared with the conventional method.

The effectiveness and superiority of the proposed fault diagnosis method are verified by experiments on PMSM. The experimental results indicate that compared with the conventional method, the proposed method possesses higher fault detection speed [within 9.7% of an electrical period)] and stronger robustness against speed change, load variation, and key parameters' errors simultaneously.

APPENDIX

The adaptive fault detection thresholds are analyzed in detail here, and switch T_1 open fault is taken as an example for analyzing.

The symbols used in the following illustration are listed first, u_d^* and u_q^* are the *d–q* current controller outputs, u_{xn}^* is phase voltage command obtained by conducting Clark and Park inverse transformation for u_d^* and u_q^*, i_{xt} is the theoretical value of phase current which is determined by phase voltage reference [see (31)], i_{dt} and i_{qt} are the theoretical motor *d–q* currents, which are obtained by (32), and i_s and i_{st} are the stator current amplitudes and their theoretical value obtained by (33) and (34), respectively.

It is known that motor currents depend on motor voltages, which are near to their reference values in a healthy system. Therefore, motor currents can be estimated according to the voltage reference and motor model. The currents estimated by this method are defined as the theoretical motor currents.

According to (2), the relationship between phase voltage reference and theoretical phase current can be written as

$$u_{xn}^* - e_a = R_s i_{xt} + (L - M)\frac{di_{xt}}{dt} \approx Z_L i_{xt} \tag{31}$$

where Z_L is the impedance of the stator winding. Ignoring the phase lag induced by inductance, the impedance can be expressed as $Z_L = \sqrt{R_s^2 + \omega_e (L-M)^2}$.

Then, the motor theoretical *d–q* currents can be written as

$$\begin{bmatrix} i_{dt} \\ i_{qt} \end{bmatrix} = \frac{2}{3} \begin{bmatrix} \cos(\theta_e) & \cos(\theta_e - \frac{2\pi}{3}) & \cos(\theta_e + \frac{2\pi}{3}) \\ -\sin(\theta_e) & -\sin(\theta_e - \frac{2\pi}{3}) & -\sin(\theta_e + \frac{2\pi}{3}) \end{bmatrix} \begin{bmatrix} i_{at} \\ i_{bt} \\ i_{ct} \end{bmatrix}. \tag{32}$$

The actual stator current amplitude is

$$i_s = \sqrt{i_d^2 + i_q^2} = \sqrt{\frac{2}{3}} \cdot \sqrt{i_a^2 + i_b^2 + {i_c}^2} \tag{33}$$

and the theoretical stator current amplitude i_{st} is

$$i_{st} = \sqrt{{i_{dt}}^2 + {i_{qt}}^2}. \tag{34}$$

With the above definitions, the adaptive thresholds are analyzed. It is well known that the switch open fault would lead to actual stator current amplitude i_s decreased. Under the effect of current closed loop, current controllers would increase the theoretic stator current amplitude i_{st} in order to increase its actual value. If the variables in the adaptive thresholds expression [$||\boldsymbol{i}||_2$,$||\hat{\boldsymbol{u}}||_2$, and $||\Delta \boldsymbol{i}||_2$ in (27) and (29)] can be replaced by i_s and i_{st}, the analysis will be much easier.

After switch T_1 open fault, the phase currents satisfy

$$\begin{cases} i_a = 0 \\ i_a + i_b + i_c = 0. \end{cases} \tag{35}$$

Therefore, variable $||\boldsymbol{i}||_2$ can be simplified as

$$||\boldsymbol{i}||_2 = \sqrt{(i_a - i_b)^2 + (i_b - i_c)^2 + (i_c - i_a)^2} = \sqrt{6} \cdot |i_b|. \tag{36}$$

Similarly, stator current amplitude i_s can be simplified as

$$i_s = \sqrt{i_a^2 + i_b^2 + {i_c}^2} = \sqrt{2}\,|i_b|\,. \tag{37}$$

According to (37), (36) can be written as

$$||\boldsymbol{i}||_2 = \frac{3\sqrt{2}}{2} \cdot i_s. \tag{38}$$

Hence, $||\boldsymbol{i}||_2$ is expressed with i_s successfully. As for the vector $\hat{\boldsymbol{u}}$, it components can be simplified as follows by substituting (31) into (16):

$$\begin{bmatrix} \hat{u}_1 \\ \hat{u}_2 \\ \hat{u}_3 \end{bmatrix} = \begin{bmatrix} u_{an}^* - u_{bn}^* - e_a + e_b \\ u_{bn}^* - u_{cn}^* - e_b + e_c \\ u_{cn}^* - u_{an}^* - e_c + e_a \end{bmatrix} = Z_L \begin{bmatrix} i_{at} - i_{bt} \\ i_{bt} - i_{ct} \\ i_{ct} - i_{at} \end{bmatrix}. \tag{39}$$

By inversing (32), theoretical phase currents can be expressed as

$$\begin{bmatrix} i_{at} \\ i_{bt} \\ i_{ct} \end{bmatrix} = \begin{bmatrix} \cos(\theta) & -\sin(\theta) \\ \cos(\theta - \frac{2\pi}{3}) & -\sin(\theta - \frac{2\pi}{3}) \\ \cos(\theta + \frac{2\pi}{3}) & -\sin(\theta + \frac{2\pi}{3}) \end{bmatrix} \begin{bmatrix} i_{dt} \\ i_{qt} \end{bmatrix}. \tag{40}$$

With (39) and (40), the variable $||\hat{\boldsymbol{u}}||_2$ can be rewritten as

$$||\hat{\boldsymbol{u}}||_2 = \frac{3\sqrt{2}}{2} Z_L \cdot i_{st}. \tag{41}$$

Thus, $||\hat{\boldsymbol{u}}||_2$ is expressed with i_{st}. As to the variable $||\Delta \boldsymbol{i}||_2$, its components can be written as follows according to (18):

$$\Delta i_j(k) = i_j(k+1) - i_j(k) \approx i_j(k+1) - g i_j(k) = u_j \tag{42}$$

where $g = \exp\{-R_s \mathrm{T_s}/(L-M)\} \approx 1$.

Therefore, $\Delta \boldsymbol{i}$ can be expressed as

$$\begin{aligned} \Delta \boldsymbol{i} = \begin{bmatrix} u_1 \\ u_2 \\ u_3 \end{bmatrix} &= \begin{bmatrix} u_{an} - e_a - (u_{bn} - e_b) \\ u_{bn} - e_b - (u_{cn} - e_c) \\ u_{cn} - e_c - (u_{an} - e_a) \end{bmatrix} \\ &= Z_L \begin{bmatrix} i_a - i_b \\ i_b - i_c \\ i_c - i_a \end{bmatrix} = Z_L \boldsymbol{i} \end{aligned} \tag{43}$$

With (38), (41), and (43), the designed adaptive thresholds can be expressed as

$$T_{h1} = T_0 + \sqrt{3} m_1 \cdot i_s + \frac{3\sqrt{2}}{2} Z_L m_2 \cdot i_{st} \tag{44}$$

$$T_{h2} = T_0 + 3\sqrt{2}(m_1 + m_3 Z_L) \cdot i_s. \tag{45}$$

From (44), it can be found that under light-load condition ($i_s \approx 0$), T_{h1} would increase with i_{st} after the fault. However, under faulty conditions, the fault detection threshold is expected to be much smaller than the fault detection index to avoid missed detection. Therefore, the increase of T_{h1} would lead to the rise of the missed detection rate.

As for the adaptive threshold T_{h2} shown in (45), it is positively correlated with i_s. Thus, T_{h2} decreases with i_s after fault, which makes the fault easier to be detected.

REFERENCES

[1] W. Wang, M. Cheng and B. Zhang, "A fault-tolerant permanent-magnet traction module for subway applications," *IEEE Trans. Power Electron.*, vol. 29, no. 4, pp. 1646–1658, Apr. 2014.

[2] A. Mohammadpour, S. Sadeghi, and L. Parsa, "A generalized fault-tolerant control strategy for five-phase PM motor drives considering star, pentagon, and pentacle connections of stator windings," *IEEE Trans. Power Electron.*, vol. 61, no. 1, pp. 63–75, Jan. 2014.

[3] X. Zhou, Y. Zhou, H. Wang, M. Lu, F. Zeng, and Y. Yu, "An improved MTPA control based on amplitude-adjustable square wave injection," *IEEE Trans. Energy Convers.*, vol. 35, no. 2, pp. 956–965, Jun. 2020.

[4] C. Cecati, A. Tommaso, and F. Genduso, "Comprehensive modeling and experimental testing of fault detection and management of a nonredundant fault-tolerant VSI," *IEEE Trans. Ind. Electron.*, vol. 62, no. 6, pp. 3945–3954, Jun. 2015.

[5] X. Zhou *et al.*, "PMSM open-phase fault-tolerant control strategy based on four-leg inverter," *IEEE Trans. Power Electron.*, vol. 35, no. 3, pp. 2799–2808, Mar. 2020.

[6] M. Trabelsi, M. Boussak, and M. Gossa, "PWM-switching pattern-based diagnosis scheme for single and multiple open-switch damages in VSI-fed induction motor drives," *ISA Trans.*, vol. 51, no. 2, pp. 333–344, Mar. 2012.

[7] B. Lu and S. K. Sharma, "A literature review of IGBT fault diagnostic and protection methods for power inverters," *IEEE Trans. Ind. Appl.*, vol. 45, no. 5, pp. 1770–1777, Sep./Oct. 2009.

[8] S. Karimi, P. Poure, and S. Saadate, "Fast power switch failure detection for fault tolerant voltage source inverters using FPGA," *IET Power Electron.,* vol. 2, no. 4, pp. 346–354, 2009.

[9] Q. T. An, L. Z. Sun, K. Zhao, and L. Sun, "Switching function model-based fast-diagnostic method of open-switch faults in inverters without sensors," *IEEE Trans. Power Electron.*, vol. 26, no. 1, pp. 119–126, Jan. 2011.

[10] M. Trabelsi, M. Boussak, P. Mestre, and M. Gossa, "An improved diagnosis technique for IGBTs open-circuit fault in PWM-VSI-fed induction motor drive," in *Proc. IEEE Int. Symp. Ind. Electron.*, 2011, pp. 2111–2117.

[11] C. Shu *et al.*, "A novel diagnostic technique for open-circuited faults of inverters based on output line-to-line voltage model," *IEEE Trans. Power Electron.*, vol. 63, no. 7, pp. 4412–4421, Jul. 2016.

[12] Y. Wang *et al.*, "A comparative study of two diagnostic methods based on switching voltage pattern for IGBTs open-circuit faults in voltage-source inverters," *J. Power Electron.*, vol. 16, no. 3, pp. 1087–1096, 2016.

[13] Z. Li *et al.*, "Fast transistor open-circuit faults diagnosis in grid-tied three-phase VSIs based on average bridge arm pole-to-pole voltages and error-adaptive thresholds," *IEEE Trans. Power Electron.*, vol. 33, no. 9, pp. 8040–8051, Sep. 2018.

[14] M. A. Rodriguez-Blanco *et al.*, "A failure-detection strategy for IGBT based on gate-voltage behavior applied to a motor drive system," *IEEE Trans. Power Electron.*, vol. 58, no. 5, pp. 1625–1633, May 2011.

[15] M. A. Rodr´ıguez-Blanco *et al.*, "Fault detection for IGBT using adaptive thresholds during the turn-on transient," *IEEE Trans. Power Electron.*, vol. 62, no. 3, pp. 1975–1983, Mar. 2015.

[16] A. M. S. Mendes and A. J. Marques Cardoso, "Voltage source inverter fault diagnosis in variable speed ac drives by the average current Park's vector approach," in *Proc. IEEE Int. Electr. Mach. Drives Conf.*, 1999, pp. 704–706.

[17] N. M. A. Freire, J. O. Estima, and A. J. M. Cardoso, "Open-circuit fault diagnosis in PMSG drives for wind turbine applications," *IEEE Trans. Ind. Electron.*, vol. 60, no. 9, pp. 3957–3967, Sep. 2013.

[18] D. Diallo, M. E. H. Benbouzid, D. Hamad, and X. Pierre, "Fault detection and diagnosis in an induction machine drive: A pattern recognition approach based on concordia stator mean current vector," *IEEE Trans. Energy Convers.*, vol. 20, no. 3, pp. 512–519, Sep. 2005.

[19] D. U. Campos-Delgado, J. A. Pecina-Sanchez, D. R. Espinoza-Trejo, and E. R. Arce-Santana, "Diagnosis of open-switch faults in variable speed drives by stator current analysis and pattern recognition," *IET Electron. Power Appl.*, vol. 7, no. 6, pp. 509–522, 2013.

[20] J. O. Estima, and A. J. Marques Cardoso, "A new approach for real-time multiple open-circuit fault diagnosis in voltage-source inverters," *IEEE Trans. Ind. Appl.*, vol. 47, no. 6, pp. 2487–2494, Nov./Dec. 2011.

[21] J. O. Estima and A. J. Marques Cardoso, "A new algorithm for real-time multiple open-circuit fault diagnosis in voltage-fed PWM motor drives by the reference current errors," *IEEE Trans. Ind. Electron.*, vol. 60, no. 8, pp. 3496–3505, Aug. 2013.

[22] J. Zhang *et al.*, "High-performance fault diagnosis in PWM voltage-source inverters for vector-controlled induction motor drives," *IEEE Trans. Power Electron.*, vol. 29, no. 11, pp. 6087–6099, Nov. 2014.

[23] F. Wu and J. Zhao, "A real-time multiple open-circuit fault diagnosis method in voltage-source-inverter fed vector controlled drives," *IEEE Trans. Power Electron.*, vol. 31, no. 2, pp. 1425–1437, Feb. 2016.

[24] S. M. Jung *et al.*, "An MRAS-based diagnosis of open-circuit fault in PWM voltage-source inverters for PM synchronous motor drive systems," *IEEE Trans. Power Electron.*, vol. 28, no. 5, pp. 2514–2526, May 2013.

[25] N. M. A. Freire, J. O. Estima, and A. J. M. Cardoso, "A voltage-based approach without extra hardware for open-circuit fault diagnosis in closed loop PWM AC regenerative drives," *IEEE Trans. Ind. Electron.*, vol. 61, no. 9, pp. 4960–4970, Sep. 2014.

[26] D. U. C. Delgado and D. R. E. Trejo, "An observer-based diagnosis scheme for single and simultaneous open-switch faults in induction motor drives," *IEEE Trans. Power Electron.*, vol. 58, no. 2, pp. 671–679, Feb. 2011.

[27] D. R. Espinoza-Trejo, D. U. Campos-Delgado, G. Bossio, E. Barcenas, J. E. Hernández-Díez, and L. F. Lugo-Cordero, "Fault diagnosis scheme for open-circuit faults in field-oriented control induction motor drives," *IET Power Electron*., vol. 6, no. 5, pp. 869–877, May 2013.

[28] Q. T An, L. Sun, and L. Z. Sun, "Current residual vector-based open switch fault diagnosis of inverters in PMSM drive systems," *IEEE Trans. Power Electron.*, vol. 30, no. 5, pp. 2814–2827, May 2015.

[29] I. Jlassi *et al.*, "Multiple open-circuit faults diagnosis in back-to-back converters of PMSG drives for wind turbine systems," *IEEE Trans. Power Electron.*, vol. 30, no. 5, pp. 2689–2702, May 2015.

[30] I. Jlassi, J. O. Estima, S. K. E. Khil, N. M. Bellaaj, and A. J. M. Cardoso, "A robust observer-based method for IGBTs and current sensors fault diagnosis in voltage-source inverters of PMSM drives," *IEEE Trans. Ind. Appl.*, vol. 53, no. 3, pp. 2894–2905, May/Jun. 2017.

[31] T. Shi *et al.*, "An improved open-switch fault diagnosis technique of a PWM voltage source rectifier based on current distortion," *IEEE Trans. Power Electron.*, vol. 34, no. 12, pp. 12212–12225, Dec. 2019.

[32] J. Fang, X. Zhou and G. Liu, "Instantaneous torque control of small inductance brushless dc motor," *IEEE Trans. Power Electron.*, vol. 27, no. 12, pp. 4952–4964, Dec. 2012.

Xinxiu Zhou (Member, IEEE) received the B.S. degree from Yanshan University, Hebei, China, in 2006, and the Ph.D. degree from Beihang University, Beijing, China, in 2013.

She is currently a lecturer with the Research Institute for Frontier Science, Beihang University. Her research interests include motor control, power electronics, and spacecraft attitude control.

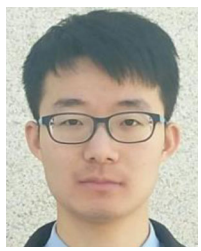

Jun Sun received the B.S. degree in detection guidance and control in 2018 from Beihang University, Beijing, China, where he is currently working toward the M.S. degree.

He is currently a Research Member of the Fundamental Science for Novel Inertial Instrument and Navigation System Technology Laboratory in Beihang University. His research interests include fault diagnosis and fault-tolerant control of permanent-magnet synchronous motor and the advanced control strategies for motor control.

Peiling Cui (Member, IEEE) was born in Henan Province, China, in 1975. She received the Ph.D. degree in control theory and control engineering from Northwestern Polytechnical University, Xi'an, China, in 2004.

She is currently an Associate Professor with the Research Institute for Frontier Science, Beihang University, Beijing, China. Her main research interests include motor control and magnetically suspended rotor control.

Yanhua Lu received the B.S. degree from the Harbin Institute of Technology, Harbin, China, in 1997, and the B.S. degree from Shanghai Normal University, Shanghai, China, in 2009.

She is currently involved in the research of servo system performance evaluation and fault detection methods and has participated in a number of servo system projects.

Ming Lu received the B.S. and M.S. degrees from Xi'an Jiao Tong University, Xi'an, China, in 2004 and 2007, respectively, and the Ph.D. degree from the Chinese Academy of Electrical Engineering, Beijing, China, in 2013.

He is currently a Senior Engineer with the Beijing Institute of Control Engineering, Beijing, China. His main research interests include high precision space actuator, active magnetic bearing, and robust control.

Yang Yu received the B.S. and M.S. degrees from the Beijing University of Chemical Technology, Beijing, China, in 2005 and 2008, respectively, and the Ph.D. degree from Beihang University, Beijing, China, in 2012.

He is currently a Research Fellow with the Faculty of Engineering and Information Technology, University of Technology Sydney, Sydney, NSW, Australia. His current research interests include data fusion, machine learning, and nonlinear modeling.